Self-assembly of Amyloid-beta (Aβ) Peptides from Solution to near in Vivo Conditions

Phuong H Nguyen, Fabio Sterpone, Philippe Derreumaux

Self-assembly of Amyloid-beta (Aβ) Peptides from Solution to near in Vivo Conditions

Phuong. H. Nguyen,[1] Fabio Sterpone,[1] Philippe Derreumaux [1,2*]

1 CNRS, Université Paris Cité, UPR 9080, Laboratoire de Biochimie Théorique, Institut de Biologie Physico-Chimique, Fondation Edmond de Rothschild, 13 rue Pierre et Marie Curie, 75005 Paris, France.

2 Institut Universitaire de France (IUF), 75005, Paris, France.

Abstract: Understanding the atomistic resolution changes during the self-assembly of amyloid peptides or proteins is important to develop compounds or conditions to alter the aggregation pathways and suppress the toxicity, and potentially aid in the development of drugs. However, the complexity of protein aggregation and the transient order/disorder of oligomers along pathways to fibril are very challenging. In this perspective, we discuss computational studies of amyloid polypeptides carried out under various conditions, including conditions closely mimicking *in vivo,* and point out the challenges in obtaining physiologically-relevant results, focusing mainly on the amyloid-beta Aβ peptides.

1.Introduction

Amyloid fibril with a cross β-structure and intermolecular H-bonds parallel to the long fibril axis is a hallmark of many sequences differing in amino acid length and composition involved in neurogenerative diseases. These involve Aβ and tau proteins in Alzheimer's disease (AD), α-synuclein in Parkinson disease, superoxide dismutase 1 (SOD1) protein in amyotrophic lateral sclerosis, transthyretin protein in cardiac and systemic amyloidosis, prion protein in prion disease, and human islet amyloid polypeptide (hIAPP) in type 2 diabetes, among others. Fragments of these proteins form fibrils as well, which represent ideal systems for computational studies.[1] In this perspective, we mainly focus on the Aβ peptides.

2. Results and Discussion

2.1. Protein self-assembly under quiescent solution conditions

The aggregation kinetics of amyloid proteins in aqueous solution, as measured by Thioflavin T (ThT) fluorescence assays, displays a sigmoidal curve with a lag-phase where monomers undergo conformational conversion and self-assemble into oligomers until the growth phase where the fibril elongates. This is followed by the saturation phase where the system is in equilibrium between fibrils and a low concentration of monomers. Aggregation is described by microscopic events involving primary nucleation, elongation and dissociation of a fibril by one monomer, and secondary (fibril fragmentation and fibril surface-catalyzed) nucleation. The rates of the different microscopic processes are obtained by fitting the experimental aggregation kinetic curves using multiple initial monomer concentrations. It was shown the aggregation kinetics is sensitive to variations in temperature, pH, protein concentration, ionic strength, and the presence of cofactors and preformed aggregates.[2]

General questions probing amyloid fibril formation of short peptides adopting straight β-strands in the bulk solution were addressed by on-lattice models and Monte Carlo simulations. It was demonstrated that the energy difference between the monomeric native state and the fibril-prone (N*) state, and therefore the population of the ensemble of N* structures in the full spectrum of conformations, are the major determinants of the time for fibril formation.[3,4] Based on a cubic lattice that considers the formation of H-bonds and pairwise side chain interactions,[5] and replica exchange Monte Carlo simulations with the OPEP force field,[6] the critical nucleus size of Aβ16-22 was estimated to be 10 monomers,[7] and the fibril state of Aβ37-42 with parallel β-strands was populated 4% for 20-mers.[8] Figure 1A shows

the free energy landscape of 10-mers Aβ37-42 as function of the nematic order parameter P2 and the number of intermolecular H-bonds at room temperature.[7] Up to 91% of states are disordered (P2 < 0.3 and N-HB < 15). The two ordered S7 and S8 states consisting of two β-sheets with populations of 2% and 1% match the experimental microcrystal structures of Aβ16-22 and Aβ37-42 fibrils,[9] indicating that the parallel and antiparallel orientations of the β-strands are encoded in the C-terminus amino acid sequence of Aβ42.

Caflisch and Shea proposed two off-lattice coarse-grained models in aqueous solution by tuning the probability of the N* monomer adopting a β-strand. Using Langevin dynamics, Caflisch et al. showed that at a concentration of 8.5 mM, the size of primary nucleus varies from 4 to 50 monomers as the function of the population of the N* state, and amyloid polymorphism is under kinetic control.[10] Using Langevin dynamics, Shea et al. demonstrated that aggregation into fibrils at a concentration of 80 mM occurs via three main mechanisms: (i) directly from the assembly of early ordered oligomers (one-step primary nucleation, 1SN), (ii) through on-pathway, nonfibrillar aggregates rich in β-sheet content, and (iii) formation of amorphous aggregates followed by reorganization to β-sheet aggregates and to fibrils (two-step primary nucleation, 2SN).[11]

Incorporating more degrees of freedom, the aggregation of Aβ16-22 peptides was followed by discrete molecular dynamics (DMD) simulations using the PRIME four-bead coarse-grained protein model with implicit solvent. Assuming 1SN mechanism, which was confirmed by electron spray ionization ion-mobility spectrometry mass spectrometry,[12] the thermodynamic phase diagram of Aβ16-22 fitted well TEM (transmission electron microscopy) fibrillation experiments at peptide concentrations varying from 10 to 200 μM at 277–330 K.[13] It is to be noted that the N- and C-terminal unprotected Aβ16-22 peptides at concentration of 30 μM and above show rapid kinetics fibrillation within seconds to minutes consistent with the nucleation-elongation 1SN and suggest a nucleus size of 6-7 peptides displaying two perpendicular β-sheets (see Figure 1B).[14] Coarse-grained OPEP Lattice-Boltzmann molecular dynamics (LBMD) simulations of 1000 Aβ16-22 peptides protected by acetyl and NH_2 with hydrodynamics also reported critical nuclei of 6-10 mers.[15] The PRIME model coupled to DMD investigated the co-aggregation of Aβ40 by Aβ16-22 and found that Aβ16-22 increases the aggregation rate of Aβ40 by a surface-catalyzed secondary nucleation mechanism.[16]

A challenging problem is the simulation of fibril formation using atomistic protein force field and explicit solvent. Bias-exchanged (BE) metadynamics with several collective variables

(CV) describing various ordered β-sheets and side chain packings revealed two distinct primary nucleation events at a concentration of 120 mM: (i) transition from mixed parallel/antiparallel to parallel β-sheets for 18 Val_8 peptides,[17] and (ii) formation of specific interdigitation of the side chains for 18 Aβ35-40 peptides.[18]

Multi-*e*Go, a recent atomistic, hybrid-structure-based model that takes advantage on the knowledge of monomers conformational ensemble in explicit solvent and of the fibril structure was developed to follow in time and at atomic resolution the primary and secondary nucleation processes of a system consisting of 4000 transthyretin 105-115 peptides. The concentration dependence of the kinetics was found consistent with ThT fluorescence assays at concentrations of 7, 10 and 13 mM. Molecular dynamics (MD) simulations in explicit solvent revealed multiple primary nuclei consisting of 10 monomers organized in two opposed β-sheets (Figure 1C) populated for less than 0.1% in the lag phase time, and secondary nucleation was the main effect contributing to the exponential growth of the fibril mass.[19]

A few studies also combined all-atom representation and coarse-grained water model. The PACE-ASM force field with an atomistic representation of the peptide and the MARTINI water model representing four water molecules by a single site was used to study the self-assembly of 18 Aβ16-22 and tau PHF6 peptides in a cubic box of 3.0 nm size. At the end of 3 and 10 μs of conventional MD at 330 K, the majority (>70%) of the Aβ16-22 and PHF6 peptides formed a double-layered filament, which each layer composed of in-register antiparallel (Aβ16-22) and parallel (PHF6) β-strands, consistent with the experimental fibrils.[20] It is unclear why the PACE-ASM-generated free energy landscape of both peptides is funnelled towards fibrillar states, as MD is sufficient to explore very rapidly fibrillar states, and peptides should spend most of their times in misregistered β-sheets.[21,22] Using the PACE force field, BE-metadynamics with multiple CVs, and cluster statistical mechanics, Han et al. showed that Aβ16-21 self-assembly follows a 2SN mechanism at 10 mM or above. At the critical oligomer concentration of 360 μM, aggregation follows a mechanism reminiscent of 1SN mechanism, but with atypical pathways characterized by growing oligomers with structured cores wrapped by disordered surfaces (Figure 1D).[23]

Much less is known on the self-assembly of full-length Aβ peptides at atomic resolution and understanding transient disorder along pathways to amyloid is a real challenge experimentally,[24,25] and computationally. It was demonstrated that the difference between Aβ42 and Aβ40 aggregation kinetics is due to a shift of more than one order of magnitude in

the relative importance of primary nucleation versus fibril-catalyzed secondary nucleation.[26] It is not clear whether our current repertoire of fibrillar U-shaped (strand-loop-strand) topology and S-shaped (three strands separated by loops) topology is complete, as cryo-electron microscopy of Aβ42 fibrils from human brains is revealing new filament types for individuals with familial Alzheimer's disease and other pathological conditions.[27] Thermodynamics of the formation of all types of Aβ amyloid fibrils from non-equilibrium experiments of growth and dissociation would be also very useful.[28] Coarse-grained (SOP-IDP) simulations determined that the N* state of Aβ2 monomer coding for the U-shaped conformation should form earlier than the N* state coding for the S-shaped conformation, and both N* states have very low populations in solution.[29] Using one particle per amino acid and lattice simulations, the critical nucleus size of Aβ40 was estimated to be 11 monomers for the U-shape conformation at a concentration of 290 μM.[30]

Saric et al. developed a simple stick-like hard spherocylinder model with attractive patches and three interaction parameters: ε-bb for two monomers interacting in the parallel β-form, ε-bs for one amyloid-competent β monomer interacting with a soluble monomer, and ε-ss for two interacting soluble monomers. Using Monte Carlo simulations at concentrations varying between 60 μM and 4mM, primary Aβ42 nucleation in aqueous solution takes place through a 2SN mechanism involving a rare oligomer size rather than the most prevalent oligomers with a primary nucleus of 7-8 peptides.[31] Using the same model, they found that secondary nucleation of Aβ40 dominates primary nucleation in a very narrow regime of inter-protein interactions.[32]

Structural characterization of Aβ40/42 oligomers in the bulk solution is still very scarce despite extensive experimental and computational studies. Visualizing and trapping transient oligomers is a real challenge.[33] This is particularly important as amyloid plaques formed by these peptides in the extracellular space have, in fact, been observed in humans not affected by Alzheimer's disease,[34] and soluble Aβ oligomers were shown to directly inhibit ubiquitin proteasome system[35] and to be the most toxic species.[36] It should be emphasized that impaired cellular processing by proteasome and autophagy was also suggested to contribute to the accumulation of toxic hIAPP.[37]

There is experimental discrepancy in the β-sheet content of oligomers, varying between 13% and 39%, as the function of the sample preparation.[38,39] Atomistic simulations on Aβ40 monomer[40] and Aβ42 dimer[41] demonstrated that the conformational ensemble

varies from one force field to another, a feature observed for many intrinsically disordered proteins and oligomers.[42-44] Simulations starting from disordered states and nuclear magnetic resonance (NMR) studies suggest small oligomers with transient antiparallel β-sheets.[45-50] For example, simulations on Aβ40 dimer using the PACE-MARTINI force field showed that the antiparallel β-sheet structure forms with a time scale of 200 μs and a probability of 1.3% and the U-shaped fibril conformation forms with a time scale of 25.8 ms and a probability of 0.02%.[48] Simulations in explicit solvent revealed β-barrel motifs in Aβ42 trimer[49] and tetramer.[50]

Recently, the AlphaFold2 method, which revolutionized structure prediction of single domain folded proteins,[51] predicted parallel α-helix bundles spanning the C-terminal residues in equilibrium with β-hairpin assemblies spanning the central hydrophobic core and part of the C-terminus in Aβ42 aggregates < 6 peptides.[52] A short α-helix spanning residues 17-23 and a 3-10 helix spanning residues 13-23 were reported for Aβ40 monomer by a predictive coarse-grained force field in solution free of salt,[53] and a NMR study at pH 7.3 with 50 mM NaCl,[54] respectively. Interestingly, circular dichroism (CD) experiments on Aβ42 peptides in pure buffer give 19% of α-helix structure after 4 days of incubation.[38] Addition of trifluoroethanol (TFE) concentrations on Aβ fibril assembly suggested partially helical intermediates,[55] and partial helical structures of Aβ40 induced by low solvent polarity accelerated amyloid fibrillation.[56] Furthermore, ThT assay and FTIR (Fourier Transform Infrared) spectroscopy on polyQ-$A\beta_{30-42}$ peptides at μM concentration suggested an aggregation mechanism initiated by a rapid formation of α-helical oligomers mediated by the C-terminal residues, in agreement with AlphaFold2 results.[57] Detection of helical intermediates during amyloid formation by intrinsically disordered peptides and proteins was also reported.[58] All these results may indicate very low population of metastable α-helix topologies that may not be detectable within the current experimental precision. Another intermediate discussed by Daggett et al. is the formation of oligomers with the nonstandard α-sheet secondary structure during the lag phase of Aβ aggregation.[59]

2.2. Protein self-assembly near in vivo conditions

The brain is composed of neural cells (neurons, astrocytes, oligodendrocytes, and microglia), the vascular system including arteries, arterioles, capillaries, venules and veins, and the interstitial system (ISS). The brain ISS, which is circumscribed by the plasma membrane of

neurons or glia, and the wall of the blood vessels, is composed of the interstitial fluid (ISF) and the extracellular matrix (ECM), and occupies 15-20% of the total brain volume. The brain ISS is an irregular, tortuous and narrow space among neural cells and capillaries. ISF includes waters, ions, gaseous molecules, and organic molecules, such as proteins, peptides, enzyme, dopamine, osmolytes, glucose, extracellular vesicles and the floating chains of glycoproteins attached to the ECM. The ECM consists of collagens, glycosaminoglycans, elastin, proteoglycans and glycoproteins (reelin, laminim, fibronectin and tesnacin).[60] Aβ peptides accumulate in the crowded extracellular space and removal of Aβ products can occur through ISF, and the cerebrospinal fluid (CSF) which fills the cerebral ventricles and the subarachnoid space.[61] In what follows we describe what experimental and computational studies tell us about Aβ-membrane interactions, and the aggregation of Aβ peptides in crowded environment and under fluid flows.

Amyloid-membrane interactions. The interaction between amyloidogenic proteins and the lipid cell membrane catalyzes *in vitro* amyloid nucleation.[62] AFM images of α-synuclein and Aβ42 revealed that self-assembly on 1-(3-aminopropyl) silatrane mica surfaces occurs at nanomolar concentrations, a concentration found for Aβ42 in human brains.[63] Cholesterol was found to enhance the primary nucleation rate of Aβ42 aggregation in the presence of lipid bilayers by up to 20-fold *in vitro*.[64] The binding of Aβ to ganglioside-containing membranes also plays an important role in the pathogenesis of AD.[65] Interactions of Aβ species and other amyloid proteins with membrane cell are very transient and oligomer-size dependent.[62,66-68] Helical intermediates appear to be particularly important in membrane-catalyzed amyloid formation.[69]

Extending their cubic lattice to interactions of Aβ42 with hydrophilic and hydrophobic surfaces, Li et al. showed that, consistent with experimental studies, an increase in roughness slows down fibril formation, and this process becomes inhibited at a very highly level of roughness.[70] Introducing a three-bead model for lipids to their protein stick model, Saric et al. identified two membrane-assisted nucleation mechanisms: (i) formation of Aβ42 oligomers on the membrane surface and subsequent nucleation into pure fibrils, and (2) stabilization of the β-prone protein conformation through hydrophobic contacts with lipids and the associated mixing of membrane lipids with fibril-forming proteins enhanced by membrane fluidity.[71]

Aβ adsorbs and interacts with lipid membranes through the carpeting effect and amyloid-pore mechanisms as assessed by TEM, EM (electron microscopy), conductance and NMR experiments.[62,72-74] Ramamoorthy et al. proposed a two-step mechanism of membrane disruption by Aβ through membrane fragmentation and pore formation.[75] Based on a variety of biophysical methods and MD simulations, La Rosa et al. proposed a lipid-chaperone hypothesis as a mechanism of protein-membrane poration.[76] Like tau oligomers, Aβ oligomers have a detergent-like activity by removing lipids from the bilayer and creating amyloid-lipid complexes.[71,77-79] Senile plaques of AD patients accumulate phospholipids, promoting the destabilization of plaques into toxic oligomers by a lipid-promoted fibril fragmentation.[80] Accumulation of cholesterol was also assessed in microdissected AD senile plaques by mass spectrometry.[81] Overall, the accumulation of free phospholipid, cholesterol and ganglioside in the ISS is most likely to modify the free energy surface of amyloid oligomers.[82-85]

Change in lipid composition of the membrane due to AD aging conditions, i.e., the amount of sphingomyelin,[86] ganglioside GM1, glycerophospholipids, and omega-3 and omega-6 polyunsatured fatty acids,[87] may also trigger amyloid toxicity in AD as assessed by *in vitro* experiments[88] and simulations.[89-91] Finally, the enhance of lipid peroxidation in brain of AD patients compared to matched-age controls[92] also changes membrane fluidity and permeability on an atomic scale by computational means.[93]

Amyloid-crowding interactions. I*n vitro*, low and high percentages of dextran70 and Ficoll400 promote and inhibit Aβ40 fibrilization, respectively.[94] Primary nucleation, fiber elongation and secondary nucleation steps of α-synuclein are accelerated by the presence of 140 and 280 mg/mL Ficoll70, while sucrose, a small-molecule osmolyte and building block of Ficoll70, slows down α-synuclein amyloid formation.[95] Ficoll70 and dextran70 also enhance tau244-372 fibrillization.[96] As a result of molecular crowding, trimethylamine-N-oxide (TMAO), a gut microbiota metabolite derived from dietary choline and carnitine, enhances Aβ aggregation kinetics.[97]

At computational level, the addition of the osmolyte TMAO shifts the atomistic conformations of tau273-286 monomer, but does not generate new conformations,[98] and favors the formation of β-strands in dimer, and tetramer of hIAPP23-29.[99] Using single-particle hard sphere crowders, a coarse-grained DMD simulation suggested that crowding increases the rate of oligomer formation and fibril growth of Aβ16-22 peptide, and this effect is crowder-size dependent at a volume crowder fraction of 0.10.[100] Using all-atom protein model for the

transthyretin fragment 105-115, implicit solvent MD simulations showed that hard sphere crowding destabilizes in-register dimeric β-sheets, but stabilizes β-sheets made of trimers and tetramers, and emphasized the influence of nanoparticle shape on protein aggregation.[101] Finally, crowding can have specific interactions with amyloid proteins favoring misfolding and competing with the aggregation. For example, a semi-unfolded intermediate SOD1 monomeric state was identified by a multi-scale simulation in a crowded BSA (bovine serum albumin) solution.[102]

Amyloid-fluid flow interactions. Using *in vivo* two-photon and *ex vivo* fluorescence imaging, Nedergard et al. showed that cerebral arterial pulsation resulting from the pulsative blood flow drives paravascular CSF-ISF exchange in the murine brain. There is a ten-fold increase in CSF tracer influx and a doubling of Aβ clearance from wake to sleep, during which the ISS volume increases by about 60% due to the fluid expelled from astrocytes.[103] Recent reports revealed that reduced sleep quality occurs with brain aging suggesting a causal relationship between sleep disturbance and progression of the neurodegenerative diseases,[104] and the sleep-wake cycle also regulates ISF tau in mice and CSF tau in humans.[105]

Both bulk flow and hindered diffusion are mechanisms of substance transport in the ISS.[106] Tortuosity (λ) and volume fraction (α) are two parameters to describe the geometry of the brain ISS. λ is the square root ratio between the diffusion coefficient in a free medium and that measured in the brain ISS. α is defined as the ratio of ISS volume to total brain volume. Increase of these two parameters was reported in the cortex in a mouse AD model.[107] Local restriction in the interstitial channels of the extracellular space, as the width of the ECS varies from 38 to 64 nm in adult rat neocortex (Figure 2A),[108,109] and interactions with cell membrane and ECM network have a significant influence on substrate transport in the ISS[106] and should generate locally different flow patterns. By analogy with computational modelling of ISF in brain tumours, accumulation of Aβ should change the properties of the flow.[110]

It is known that extensional flows caused by a gradient in velocity in the direction of travel induce protein aggregation of BSA in microfluidic devices (Figure 2B) by inducing partial unfolding.[111] Aggregation kinetics of Aβ40 in a Couette cell (Figure 2C), that is subject to a shear flow generated by a gradient in velocity perpendicular to the direction of travel, showed that increased shear rates decrease the lag phase time, increase the growth rate and the final concentration of fibrils (Figure 2D). It was shown that the addition of a depolymerization event

(leading to the formation of a monomer and a (i-1) fibril)) to primary and secondary nucleation and elongation steps suffices to reproduce the time evolution of fibril concentrations at different shear rates.[112] Similar kinetics behaviour was reported for Aβ42 under fluid flows.[113]

While shear-induced monomeric protein dynamics were explored by experimental[114,115] and computational[116-120] studies, and lipid systems were also investigated under shear flows,[121-124] we still lack an atomic description of Aβ aggregates under fluid flows in the bulk solution and at the surface of membranes. Yet is it known that flowing acting on the membrane surface showed desorption, diffusion and collision of Aβ-lipid aggregates forming larger plaque-like aggregates.[125] Overall, hydrodynamic flow fields in ISS are likely to change the conformational ensemble states assessed by small Aβ oligomers and may promote very rare excited oligomers.[126]

3. Conclusions

In summary, we are gaining a better atomistic description of the aggregation of short amyloid peptides in the bulk solution. Whether all relevant oligomeric microstates with α-helix and β-barrel[127-130] contents or associated with multiple strains[131] are sampled correctly by current simulations remains to be determined.

It is a real challenge to characterize the relevant physical and pathological conformations of Aβ40/42 oligomers in the bulk solution or at the membrane cells as they are likely to be marginally populated. Results are likely to depend on the force field and the membrane composition. Metadynamics simulations in the bulk solution of small Aβ40/42 oligomers with CVs featuring α-helix, α-sheet,[59] misregistered β-sheets, α-helix bundles[52] and β-barrels[132] could identify population and structures of rare aggregates. Path sampling simulations may also reveal unexpected excited states.[133] These simulations could be followed by the development of a Markov state model to characterize the kinetics between on-pathway and off-pathway oligomers and the role of water mobility in the early steps of aggregation.[134] The concentration-dependence of aggregation pathways and oligomers at nM concentrations or lower as it is observed for Aβ40/42 peptides in human brains has also to be considered,[135] and liquid-liquid phase separations may help in this context.

There is still a very large gap between simulations and *in vivo* conditions. Constant progress regarding the interactions of amyloid oligomers with membranes is noted and experimental data may guide simulations to further explore the conformational ensemble.[136]

Simulations under crowding conditions are far behind, and going from *in vitro* to *in vivo* observations is not an easy task.[137] Simulations based on implicit solvent models without hydrodynamics effects cannot capture, however, the size fluctuations of the oligomers.[138,139] Furthermore, the role of crowding is far of being evident as human CSF, which contains antibodies, albumin, fibrinogen among others, delays Aβ40/42 aggregation under quiescent conditions.[140,141]

Finally, coarse-grained simulations, taking into account the non-regular and tortuous geometry and the alterations of the ISS space, crowding including prion protein and NMDA receptor, and fluid flow variations during sleep-wake cycle could unveil unexpected phenomena and aggregates. More elaborated microfluidic experiments could also approach *in vivo* conditions.[120,125,142] These combined studies could help design more efficient drugs targeting Aβ monomer and oligomers.[135,143]

AUTHOR INFORMATION

Corresponding Author

E-mail: philippe.derreumaux@ibpc.fr

ORCID:

Derreumaux: 0000-0001-9110-5585, philippe.derreumaux@ibpc

Sterpone: 0000-0003-0894-8069, fabio.sterpone@ibpc.fr

Nguyen: 0000-0003-1284-967X, phuong.nguyen@ibpc.fr

Biographies

Phuong H. Nguyen is a CNRS Researcher at the Laboratoire de Biochimie Théorique at the Institut de Biologie Physico-Chimique (IBPC) in Paris. He received his M.Sc. from ICTP, Italy, and his Ph.D. from the University of Bielefeld, Germany, in Theoretical Condensed Matter Physics. He was then a Postdoctoral Fellow at the University of Frankfurt. His current research focuses on the development and application of theoretical methods for studying equilibrium and nonequilibrium structure, dynamics, and thermodynamics of single proteins, amyloids, and membranes at all-atom and coarse-grained levels.

Fabio Sterpone is a Research Director at the CNRS, and works at the Laboratoire de Biochimie Théorique at IBPC in Paris. He graduated from the University of Paris UPMC (biophysics). He has a broad experience in the application and development of computational methods to soft-matter systems. Presently, he is mainly interested in the study of protein stability and aggregation by applying and developing multiscale simulation methodologies.

Philippe Derreumaux is Professor at Université Paris Cité and Senior Member of the Institut Universitaire de France. He has been working at IBPC on the development of coarse-grained

protein model, peptide structure prediction, and the self-assembly of amyloid proteins in various environments by computer simulations.

Notes

The authors declare no competing financial interest.

ACKNOWLEDGMENTS

This work was supported by the “Initiative d’Excellence” program from the French State, Grant “DYNAMO”, ANR-11-LABX-0011.

REFERENCES

1.Dobson, C.M. Protein Folding and Misfolding. *Nature.* **2003**, *426*, 884-890.
2. Knowles, T.P.; Waudby, C.A.; Devlin, G.L.; Cohen, S.I.; Aguzzi, A.; Vendruscolo, M.; Terentjev, E.M.; Welland, M.E.; Dobson, C.M. An Analytical Solution to the Kinetics of Breakable Filament Assembly. *Science.* **2009**, *326*, 1533-1537.
3. Li, M.S.; Co, N.T.; Reddy, G.; Hu, C.K.; Straub, J.E.; Thirumalai, D. Factors Governing Fibrillogenesis of Polypeptide Chains Revealed by Lattice Models. *Phys Rev Lett.* **2010,** *105*, 218101.
4. Li, M.S.; Klimov, D.K.; Straub, J.E.; Thirumalai, D. Probing the Mechanisms of Fibril Formation using Lattice Models*. J Chem Phys.* **2008**, *129*, 175101.
5. Abeln, S.; Vendruscolo, M.; Dobson, C.M.; Frenkel, D. A Simple Lattice Model that Captures Protein Folding, Aggregation and Amyloid Formation. *PLoS One.* **2014,** *9*, e85185.
6. Sterpone, F. ; Melchionna, S. ; Tuffery, P. ; Pasquali, S. ; Mousseau, N. ; Cragnolini, T. ; Chebaro, Y. ; St-Pierre, J.F. ; Kalimeri, M. ; Barducci, A. et al. The OPEP Protein Model: From Single Molecules, Amyloid Formation, Crowding and Hydrodynamics to DNA/RNA Systems. *Chem Soc Rev.* **2014**, *43*, 4871-4893.
7. Tran, T.T.; Nguyen, P.H.; Derreumaux, P. Lattice Model for Amyloid Peptides: OPEP Force Field Parametrization and Applications to the Nucleus Size of Alzheimer's Peptides. *J Chem Phys.* **2016**, *144*, 205103.
8. Sterpone, F.; Doutreligne, S.; Tran, T.T.; Melchionna, S.; Baaden, M.; Nguyen, P.H.; Derreumaux, P. Multi-scale Simulations of Biological Systems using the OPEP Coarse-grained Model. *Biochem Biophys Res Commun.* **2018**, *498*, 296-304.
9. Sawaya, M.R.; Sambashivan, S.; Nelson, R.; Ivanova, M.I.; Sievers, S.A.; Apostol, M.I.; Thompson, M.J.; Balbirnie, M.; Wiltzius, J.J.; McFarlane, H.T. et al. Atomic Structures of Amyloid Cross-beta Spines Reveal Varied Steric Zippers. *Nature.* **2007**, *447*, 453-457.
10. Pellarin, R.; Schuetz, P.; Guarnera, E.; Caflisch, A. Amyloid Fibril Polymorphism is Under Kinetic Control. *J Am Chem Soc.* **2010**, 132, 14960-14970.
11. Bellesia, G.; Shea, J.E. Effect of Beta-sheet Propensity on Peptide Aggregation. *J Chem Phys.* **2009**, *130*, 145103.
12. Bunce, S.J.; Wang, Y.; Radford, S.E.; Wilson, A.J.; Hall, C.K. Structural Insights into Peptide Self-assembly using Photo-induced Crosslinking Experiments and Discontinuous Molecular Dynamics. *AIChE J.* **2021**, *67*, e17101.
13. Wang, Y.; Bunce, S.J.; Radford, S.E.; Wilson, A.J.; Auer, S.; Hall, C.K. Thermodynamic Phase Diagram of Amyloid-β (16-22) Peptide. *Proc Natl Acad Sci U S A.* **2019,** *116*, 2091-2096.
14. Yamazaki, M.; Ikeda, K.; Kameda, T.; Nakao, H.; Nakano, M. Kinetic Mechanism of Amyloid-β-(16-22) Peptide Fibrillation. *J Phys Chem Lett.* **2022**, *13*, 6031-6036.

15. Chiricotto, M.; Melchionna, S.; Derreumaux, P.; Sterpone, F. Multiscale Aggregation of the Amyloid $A\beta_{16-22}$ Peptide: From Disordered Coagulation and Lateral Branching to Amorphous Prefibrils. *J Phys Chem Lett.* **2019**, *10*, 1594-1599.
16. Bunce, S.J.; Wang, Y.; Stewart, K.L.; Ashcroft, A.E.; Radford, S.E.; Hall, C.K.; Wilson, A.J. Molecular Insights into the Surface-catalyzed Secondary Nucleation of Amyloid-β_{40} ($A\beta_{40}$) by the Peptide Fragment $A\beta_{16-22}$. *Sci Adv.* **2019**, *5*, eaav8216.
17. Baftizadeh, F.; Biarnes, X.; Pietrucci, F.; Affinito, F.; Laio A. Multidimensional View of Amyloid Fibril Nucleation in Atomistic Detail. *J Am Chem Soc.* **2012**, *134*, 3886-3894.
18. Baftizadeh, F.; Pietrucci, F.; Biarnés, X.; Laio, A. Nucleation Process of a Fibril Precursor in the C-terminal Segment of Amyloid-β. *Phys Rev Lett.* **2013**, *110*, 168103.
19. Scalone, E.; Broggini, L.; Visentin, C.; Erba, D.; Bačić Toplek, F.; Peqini, K.; Pellegrino, S.; Ricagno, S.; Paissoni, C.; Camilloni, C. Multi-eGO: An in Silico Lens to Look into Protein Aggregation Kinetics at Atomic Resolution. *Proc Natl Acad Sci U S A.* **2022**, *119*, e2203181119.
20. Cai, X.; Han, W. Development of a Hybrid-Resolution Force Field for Peptide Self-Assembly Simulations: Optimizing Peptide-Peptide and Peptide-Solvent Interactions. *J Chem Inf Model.* **2022**, *62*, 2744-2760.
21. Nguyen, P., Derreumaux, P. Understanding Amyloid Fibril Nucleation and Aβ Oligomer/drug Interactions from Computer Simulations. *Acc Chem Res.* **2014**, *47*, 603-611.
22. Jia, Z.; Schmit, J.D.; Chen, J. Amyloid Assembly is Dominated by Misregistered Kinetic Traps on an Unbiased Energy Landscape. *Proc Natl Acad Sci U S A.* **2020**, *117*, 10322-10328.
23. Tang, X.; Han, W. Multiscale Exploration of Concentration-Dependent Amyloid-β(16-21) Amyloid Nucleation. *J Phys Chem Lett.* **2022,** *13*, 5009-5016.
24. Morgan, G.J. Transient Disorder Along Pathways to Amyloid. *Biophys Chem.* **2022**, *281*, 106711.
25. Majumdar, A. Mukhopadhyay, S. Excitation Energy Migration to Study Protein Oligomerization and Amyloid Formation. *Biophys Chem.* **2022**, *281*, 106719.
26. Meisl, G.; Yang, X.; Hellstrand, E.; Frohm, B.; Kirkegaard, JB.; Cohen, S.I.; Dobson, C.M; Linse, S.; Knowles, T.P. Differences in Nucleation Behavior Underlie the Contrasting Aggregation Kinetics of the Aβ40 and Aβ42 Peptides. *Proc Natl Acad Sci U S A.* **2014**, *111*, 9384-9389.
27. Yang, Y.; Arseni, D.; Zhang, W.; Huang, M.; Lövestam, S.; Schweighauser, M.; Kotecha, A.; Murzin, A.G.; Peak-Chew, S.Y., Macdonald, J. et al. Cryo-EM Structures of Amyloid-β42 Filaments from Human Brains. *Science.* **2022**, *375*, 167-172.
28. Norrild, R.K.; Vettore, N.; Coden, A.; Xue, W.F.; Buell, A.K. Thermodynamics of Amyloid Fibril Formation from Non-equilibrium Experiments of Growth and Dissociation. *Biophys Chem.* **2021**, *271*, 106549.
29. Chakraborty, D.; Straub, J.E.; Thirumalai, D. Differences in the Free Energies between the Excited States of A*β*40 and A*β*42 Monomers Encode their Aggregation Propensities. *Proc Natl Acad Sci U S A.* **2020**, *117*, 19926-19937.
30. Co, N.T.; Li, M.S. New Method for Determining Size of Critical Nucleus of Fibril Formation of Polypeptide Chains. *J Chem Phys.* **2012,** *137*, 095101.
31. Šarić, A.; Chebaro, Y.C.; Knowles, T.P.; Frenkel, D. Crucial Role of Nonspecific Interactions in Amyloid Nucleation. *Proc Natl Acad Sci U S A.* **2014**, 111, 17869-17874.
32. Šarić, A.; Buell, A.K.; Meisl, G.; Michaels, T.C.T.; Dobson, C.M.; Linse, S.; Knowles, T.P.J.; Frenkel, D. Physical Determinants of the Self-replication of Protein Fibrils. *Nat Phys.* **2016**, *12*, 874-880.

33. Cawood, E.E.; Karamanos, T.K.; Wilson, A.J.; Radford, S.E. Visualizing and Trapping Transient Oligomers in Amyloid Assembly Pathways. *Biophys Chem.* **2021**, *268*, 106505.
34. Katzman, R.; Terry, R.; DeTeresa, R.; Brown, T.; Davies, P.; Fuld, P., Renbing, X.; Peck, A. Clinical, Pathological, and Neurochemical Changes in Dementia: A Subgroup with Preserved Mental Status and Numerous Neocortical Plaques. *Ann Neurol.* **1988**, *23*, 138-44.
35. Deger, J.M.; Gerson, J.E.; Kayed, R. The Interrelationship of Proteasome Impairment and Oligomeric Intermediates in Neurodegeneration. *Aging Cell.* **2015**, *14*, 715-724.
36. Selkoe, D.J.; Hardy, J. The Amyloid Hypothesis of Alzheimer's Disease at 25 Years. *EMBO Mol Med.* **2016**, *8*, 595-608.
37. Milardi, D.; Gazit, E.; Radford, S.E.; Xu, Y.; Gallardo, R.U.; Caflisch, A.; Westermark, G.T.; Westermark, P.; Rosa, C.; Ramamoorthy; A. Proteostasis of Islet Amyloid Polypeptide: A Molecular Perspective of Risk Factors and Protective Strategies for Type II Diabetes. *Chem Rev.* **2021**, *121*, 1845-1893.
38. Kirkitadze, M.D.; Condron, M.M.; Teplow, D.B. Identification and Characterization of Key Kinetic Intermediates in Amyloid Beta-protein Fibrillogenesis. *J Mol Biol.* **2001**, *312*, 1103-1119.
39. Ono, K.; Condron, M.M.; Teplow, D.B. Structure-neurotoxicity Relationships of Amyloid Beta-protein Oligomers. *Proc Natl Acad Sci U S A.* **2009**, *106*, 14745-14750.
40. Paul, A.; Samantray, S.; Anteghini, M.; Khaled, M.; Strodel, B. Thermodynamics and Kinetics of the Amyloid-β Peptide Revealed by Markov State Models based on MD Data in Agreement with Experiment. *Chem Sci.* **2021**, *12*, 6652-6669.
41. Man VH, Nguyen PH, Derreumaux P. High-Resolution Structures of the Amyloid-β 1-42 Dimers from the Comparison of Four Atomistic Force Fields. *J Phys Chem B.* **2017**, *121*, 5977-5987.
42. Man, V.H.; He, X.; Derreumaux, P.; Ji, B.; Xie, X.Q.; Nguyen, P.H.; Wang, J. Effects of All-Atom Molecular Mechanics Force Fields on Amyloid Peptide Assembly: The Case of $A\beta_{16-22}$ Dimer. *J Chem Theory Comput.* **2019**, *15*, 1440-1452.
43. Nguyen, P.H.; Derreumaux, P. Structures of the Intrinsically Disordered Aβ, tau and α-synuclein Proteins in Aqueous Solution from Computer Simulations. *Biophys Chem.* **2020**, *264*, 106421.
44. Samantray, S.; Yin, F.; Kav, B.; Strodel, B. Different Force Fields Give Rise to Different Amyloid Aggregation Pathways in Molecular Dynamics Simulations. *J Chem Inf Model.* **2020**, *60*, 6462-6475.
45. Nasica-Labouze, J.; Nguyen, P.H.; Sterpone, F.; Berthoumieu, O.; Buchete, N.V.; Coté, S.; De Simone, A.; Doig, A.J.; Faller, P.; Garcia, A. et al. Amyloid β Protein and Alzheimer's Disease: When Computer Simulations Complement Experimental Studies. *Chem. Rev.* **2015**, *115*, 3518-3563.
46. Ahmed, M.; Davis, J.; Aucoin, D.; Sato, T.; Ahuja, S.; Aimoto, S.; Elliott, J.I.; Van Nostrand, W.E.; Smith, S.O. Structural Conversion of Neurotoxic Amyloid-beta(1-42) Oligomers to Fibrils. *Nat Struct Mol Biol.* **2010**, *17*, 561-567.
47. Lendel, C.; Bjerring, M.; Dubnovitsky, A.; Kelly, RT.; Filippov, A.; Antzutkin, O.N.; Nielsen, N.C.; Härd, T. A Hexameric Peptide Barrel as Building Block of Amyloid-β Protofibrils. *Angew Chem Int Ed Engl.* **2014**, *53*, 12756-12760.
48. Cao, Y., Jiang, X.; Han, W. Self-Assembly Pathways of β-Sheet-Rich Amyloid-β(1-40) Dimers: Markov State Model Analysis on Millisecond Hybrid-Resolution Simulations. *J Chem Theory Comput.* **2017**, *13*, 5731-5744.

49. Nguyen, H.L.; Linh, H.Q.; Matteini, P.; La Penna, G.; Li, M.S. Emergence of Barrel Motif in Amyloid-β Trimer: A Computational Study. *J Phys Chem B.* **2020**, *124*, 10617-10631.
50. Nguyen, P.H., Campanera, J.M.; Ngo, S.T.; Loquet, A.; Derreumaux, P. Tetrameric Aβ40 and Aβ42 β-Barrel Structures by Extensive Atomistic Simulations. II. In Aqueous Solution*. J Phys Chem B.* **2019**, *123*, 6750-6756.
51. Jumper, J.; Evans, R.; Pritzel, A.; Green, T.; Figurnov, M.; Ronneberger, O.; Tunyasuvunakool, K.; Bates, R.; Žídek, A.; Potapenko, A., et al. Highly Accurate Protein Structure Prediction with AlphaFold. *Nature.* **2021,** *596*, 583-589.
52. Santuz, H. Nguyen, P.H.; Sterpone, F.; Derreumaux, P. Small Oligomers of Aβ42 Protein in the Bulk Solution with AlphaFold2. *ACS Chem Neurosci.* **2022**, *13*, 711-713.
53. Zheng, W.; Tsai, M.Y.; Chen, M.; Wolynes, P.G. Exploring the Aggregation Free Energy Landscape of the Amyloid-β protein (1-40). *Proc Natl Acad Sci U S A.* **2016**, *113*, 11835-11840.
54. Vivekanandan, S.; Brender, J.R.; Lee, S.Y.; Ramamoorthy, A. A Partially Folded Structure of Amyloid-beta(1-40) in an Aqueous Environment. *Biochem Biophys Res Commun.* **2011**, *411*, 312-316.
55. Fezoui, Y.; Teplow, D.B. Kinetic Studies of Amyloid Beta-protein Fibril Assembly. Differential Effects of Alpha-helix Stabilization. *J Biol Chem.* **2002**, *277*, 36948-36954.
56. Lin, Y.; Sahoo, B.R.; Ozawa, D.; Kinoshita, M.; Kang, J.; Lim, M.H.; Okumura, M.; Huh, Y.H.; Moon, E.; Jang, J.H. et al. Diverse Structural Conversion and Aggregation Pathways of Alzheimer's Amyloid-β (1-40). *ACS Nano.* **2019**, *13*, 8766-8783.
57. Misra, P.; Kodali, R.; Chemuru, S.; Kar, K.; Wetzel, R. Rapid α-oligomer Formation Mediated by the Aβ C Terminus Initiates an Amyloid Assembly Pathway. *Nat Commun.* **2016**, *7*, 12419.
58. Abedini, A.; Cao, P.; Raleigh, D.P. Detection of Helical Intermediates During Amyloid Formation by Intrinsically Disordered Polypeptides and Proteins. *Methods Mol Biol.* **2016**, *1345*, 55-66.
59. Shea, D.; Hsu, C.C.; Bi, T.M.; Paranjapye, N.; Childers, M.C.; Cochran, J.; Tomberlin, C.P.; Wang, L.; Paris, D.; Zonderman, J. et al. α-Sheet Secondary Structure in Amyloid β-peptide Drives Aggregation and Toxicity in Alzheimer's Disease. *Proc Natl Acad Sci U S A.* **2019**, *116*, 8895-8900.
60. Lei, Y.; Han, H.; Yuan, F.; Javeed, A.; Zhao, Y. The brain Interstitial System: Anatomy, Modeling, in Vivo Measurement, and Applications. *Prog Neurobiol*. **2017**, *157*, 230-246.
61. Shetty, A.K.; Zanirati, G. The Interstitial System of the Brain in Health and Disease. *Aging Dis.* **2020,** *11*, 200-211.
62. Nguyen, P.H.; Ramamoorthy, A.; Sahoo, B.R.; Zheng, J.; Faller, P.; Straub, J.E.; Dominguez, L.; Shea, J.E.; Dokholyan; N.V.; De Simone, A. et al. Amyloid Oligomers: A Joint Experimental/ Computational Perspective on Alzheimer's Disease, Parkinson's Disease, Type II Diabetes, and Amyotrophic Lateral Sclerosis. *Chem Rev.* **2021**, *121*, 2545-2647.
63. Banerjee, S.; Hashemi, M.; Lv, Z.; Maity, S.; Rochet, J.C.; Lyubchenko, Y.L. A Novel Pathway for Amyloids Self-assembly in Aggregates at Nanomolar Concentration Mediated by the Interaction with Surfaces. *Sci. Rep.* **2017**, *7*, 45592.
64. Habchi, J.; Chia, S.; Galvagnion, C.; Michaels, T.C.T.; Bellaiche, M.M.J.; Ruggeri, F.S.; Sanguanini, M.; Idini, I.; Kumita, J.R.; Sparr, E et al. Cholesterol Catalyses Aβ42 Aggregation through a Heterogeneous Nucleation Pathway in the Presence of Lipid Membranes. *Nat. Chem.* **2018**, *10*, 673-683.
65. Matsuzaki, K. Aβ-ganglioside Interactions in the Pathogenesis of Alzheimer's Disease. *Biochim Biophys Acta Biomembr.* **2020**, *1862*, 183233.

66. Fatafta, H.; Khaled, M.; Owen, M.C.; Sayyed-Ahmad, A.; Strodel, B. Amyloid-β Peptide Dimers Undergo a Random Coil to β-sheet Transition in the Aqueous Phase but not at the Neuronal Membrane. *Proc Natl Acad Sci U S A.* **2021**, *118*, e2106210118.
67. Nguyen, P.H.; Derreumaux, P. Molecular Dynamics Simulations of the Tau R3-R4 Domain Monomer in the Bulk Solution and at the Surface of a Lipid Bilayer Model. *J Phys Chem B.* **2022**, *126,* 3431-3438.
68. Nguyen, P.H.; Derreumaux, P. Molecular Dynamics Simulations of the Tau Amyloid Fibril Core Dimer at the Surface of a Lipid Bilayer Model: I. In Alzheimer's Disease. *J Phys Chem B.* **2022**, *126*, 4849-4856.
69. Abedini, A.; Raleigh, D.P. A Critical Assessment of the Role of Helical Intermediates in Amyloid Formation by Natively Unfolded Proteins and Polypeptides. *Protein Eng Des Sel.* **2009**, *22*, 453-459.
70. Co, N.T.; Li, M.S. Effect of Surface Roughness on Aggregation of Polypeptide Chains: A Monte Carlo Study. *Biomolecules* **2021**, *11*, 596.
71. Krausser, J.; Knowles, T.P.J., Šarić, A. Physical Mechanisms of Amyloid Nucleation on Fluid Membranes. *Proc Natl Acad Sci U S A.* **2020**, *117,* 33090-33098.
72. Quist, A.; Doudevski, I.; Lin, H.; Azimova, R.; Ng, D.; Frangione, B.; Kagan, B.; Ghiso, J.; Lal, R. Amyloid Ion Channels: A Common Structural Link for Protein-misfolding Disease. *Proc. Natl. Acad. Sci. U. S. A* **2005**, *102*, 10427-10432.
73. Österlund, N.; Moons, R.; Ilag, L.L.; Sobott, F.; Gräslund, A. Native Ion Mobility-Mass Spectrometry Reveals the Formation of β-Barrel Shaped Amyloid-β Hexamers in a Membrane-Mimicking Environment. *J. Am. Chem. Soc.* **2019,** *141*, 10440-10450.
74. Ciudad, S.; Puig, E.; Botzanowski, T.; Meigooni, M.; Arango, A.S.; Do, J.; Mayzel, M.; Bayoumi, M.; Chaignepain, S.; Maglia, G. et al. Aβ(1-42) Tetramer and Octamer Structures Reveal Edge Conductivity Pores as a Mechanism for Membrane Damage. *Nat. Commun*. **2020**, *11*, 3014.
75. Sciacca, M.F.; Kotler, S.A.; Brender, J.R.; Chen, J.; Lee, D.K.; Ramamoorthy, A. Two-step Mechanism of Membrane Disruption by Aβ through Membrane Fragmentation and Pore Formation. *Biophys J.* **2012**, *103*, 702-710.
76. Sciacca, M.F.; Lolicato, F.; Tempra, C.; Scollo, F.; Sahoo, B.R.; Watson, M.D.; García-Viñuales, S.; Milardi; D.; Raudino, A.; Lee, J.C. et al. Lipid-Chaperone Hypothesis: A Common Molecular Mechanism of Membrane Disruption by Intrinsically Disordered Proteins. *ACS Chem Neurosci*. **2020**, *11*, 4336-4350.
77. Ait-Bouziad, N.; Lv, G.; Mahul-Mellier, A.L.; Xiao, S.; Zorludemir, G.; Eliezer, D.; Walz, T.; Lashuel, H.A. Discovery and Characterization of Stable and Toxic Tau/phospholipid Oligomeric Complexes. *Nat. Commun.* **2017**, *8*, 1678.
78. Bera, S.; Gayen, N.; Mohid, S.A.; Bhattacharyya, D.; Krishnamoorthy, J.; Sarkar, D.; Choi, J.; Sahoo, N.; Mandal, A.K.; Lee, D.; Bhunia, A. Comparison of Synthetic Neuronal Model Membrane Mimics in Amyloid Aggregation at Atomic Resolution. *ACS Chem Neurosci.* **2020**, *11*, 1965-1977.
79. Tempra, C.; Scollo, F.; Pannuzzo, M.; Lolicato, F.; La Rosa, C. A Unifying Framework for Amyloid-mediated Membrane Damage: The Lipid-chaperone Hypothesis. *Biochim Biophys Acta Proteins Proteom.* **2022**, *1870*, 140767.
80. Sanderson, J.M. The Association of Lipids with Amyloid Fibrils. *J Biol Chem.* **2022**, *298*, 102108.

81. Panchal, M.; Loeper, J.; Cossec, J.C.; Perruchini, C.; Lazar, A.; Pompon, D.; Duyckaerts, C. Enrichment of Cholesterol in Microdissected Alzheimer's Disease Senile Plaques as Assessed by Mass Spectrometry. *J. Lipid Res.* **2010**, *51*, 598-605.
82. Ngo, S.T.; Nguyen, P.H.; Derreumaux, P. Cholesterol Molecules Alter the Energy Landscape of Small Aβ1-42 Oligomers. *J Phys Chem B.* **2021**, *125*, 2299-2307.
83. Nguyen, T.H.; Nguyen, P.H.; Ngo, S.T.; Derreumaux, P. Effect of Cholesterol Molecules on Aβ1-42 Wild-Type and Mutants Trimers. *Molecules.* **2022**, *27*, 1395.
84. Fatafta, H.; Kav, B.; Bundschuh, B.F.; Loschwitz, J.; Strodel, B. Disorder-to-order Transition of the Amyloid-β Peptide upon Lipid Binding. *Biophys Chem.* **2022**, *280*, 106700.
85. Chakravorty, A.; McCalpin, S.D.; Sahoo, B.R.; Ramamoorthy, A.; Brooks, C.L. 3rd. Free Gangliosides Can Alter Amyloid-β Aggregation. *J Phys Chem Lett.* **2022**, *13*, 9303-9308.
86. Pettegrew, J.W.; Panchalingam, K.; Hamilton, R.L.; McClure, R.J. Brain Membrane Phospholipid Alterations in Alzheimer's Disease. *Neurochem Res.* **2001**, *26*, 771-782.
87. Chew, H.; Solomon, V.A.; Fonteh, A.N. Involvement of Lipids in Alzheimer's Disease Pathology and Potential Therapies. *Front Physiol.* **2020**, *11*, 598.
88. Drolle, E.; Negoda, A.; Hammond, K.; Pavlov, E.; Leonenko, Z. Changes in Lipid Membranes May Trigger Amyloid Toxicity in Alzheimer's Disease. *PLoS One.* **2017**, *12*, e0182194.
89. Owen, M.C.; Kulig, W.; Poojari, C.; Rog, T.; Strodel, B. Physiologically-relevant Levels of Sphingomyelin, but not GM1, Induces a β-sheet-rich Structure in the Amyloid-β(1-42) Monomer. *Biochim Biophys Acta Biomembr.* **2018**, *1860*, 1709-1720.
90. Zhou, H.; Liu, S.; Shao, Q.; Ma, D.; Yang, Z.; Zhou, R. Mechanism by which DHA Inhibits the Aggregation of KLVFFA Peptides: A Molecular Dynamics Study. *J Chem Phys.* **2018**, *148*, 115102.
91. Lu, Y.; Shi, X.F.; Nguyen, P.H.; Sterpone, F.; Salsbury, F.R. Jr; Derreumaux, P. Amyloid-β(29-42) Dimeric Conformations in Membranes Rich in Omega-3 and Omega-6 Polyunsaturated Fatty Acids. *J Phys Chem B.* **2019**, *123*, 2687-2696.
92. Montine, T.J.; Neely, M.D.; Quinn, J.F.; Beal, M.F.; Markesbery, W.R.; Roberts, L.J.; Morrow, J.D. Lipid Peroxidation in Aging Brain and Alzheimer's Disease. *Free Radic Biol Med.* **2002**, *33*, 620-626.
93. Van der Paal, J; Neyts, E.C.; Verlackt, C.C.W; Bogaerts, A. Effect of Lipid Peroxidation on Membrane Permeability of Cancer and Normal Cells Subjected to Oxidative Stress. *Chem Sci.* **2016,** *7*, 489-498.
94. Lee, C.F.; Bird, S.; Shaw, M.; Jean, L.; Vaux, D.J. Combined Effects of Agitation, Macromolecular Crowding, and Interfaces on Amyloidogenesis. *J Biol Chem*. **2012**, *287*, 38006-38019.
95. Horvath, I; Kumar, R.; Wittung-Stafshede, P. Macromolecular Crowding Modulates α-Synuclein Amyloid Fiber Growth. *Biophys J.* **2021**, *120*, 3374-3381.
96. Ma, Q; Fan, J.B.; Zhou, Z.; Zhou, B.R.; Meng, S.R.; Hu, J.Y.; Chen, J.; Liang, Y. The Contrasting Effect of Macromolecular Crowding on Amyloid Fibril Formation. *PLoS One*. **2012**, *7*, e36288.
97. Buawangpong, N.; Pinyopornpanish, K.; Siri-Angkul, N.; Chattipakorn, N.; Chattipakorn, S.C. The Role of Trimethylamine-N-Oxide in the Development of Alzheimer's Disease. *J Cell Physiol.* **2022**, *237*, 1661-1685.
98. Levine, Z.A.; Larini, L.; LaPointe, N.E.; Feinstein, S.C.; Shea, J.E. Regulation and Aggregation of Intrinsically Disordered Peptides. *Proc Natl Acad Sci U S A*. **2015**, *112*, 2758-2763.
99. Khan, A.; Nayeem, S.M. Effect of TMAO and Urea on Dimers and Tetramers of Amyloidogenic Heptapeptides (^{23}FGAILSS^{29}). *ACS Omega.* **2020**, *5*, 26986-26998.

100. Latshaw, D.C.; Cheon, M.; Hall, C.K. Effects of Macromolecular Crowding on Amyloid beta (16-22) Aggregation using Coarse-grained Simulations. *J Phys Chem B*. **2014***, 118*, 13513-13526.
101. O'Brien, E.P.; Straub, J.E.; Brooks, B.R.; Thirumalai, D. Influence of Nanoparticle Size and Shape on Oligomer Formation of an Amyloidogenic Peptide. *J Phys Chem Lett.* **2011**, *2,* 1171-1177.
102. Timr, S. Gnutt, D.; Ebbinghaus, S.; Sterpone, F. The Unfolding Journey of Superoxide Dismutase 1 Barrels under Crowding: Atomistic Simulations Shed Light on Intermediate States and Their Interactions with Crowders*. J Phys Chem Lett.* **2020,** *11*, 4206-4212.
103. Iliff, J.J.; Wang, M.; Zeppenfeld, D.M.; Venkataraman, A.; Plog, B.A.; Liao, Y.; Deane, R.; Nedergaard, M. Cerebral Arterial Pulsation Drives Paravascular CSF-interstitial Fluid Exchange in the Murine Brain. *J Neurosci.* **2013**, *33*, 18190-18199.
104. Nedergaard, M.; Goldman, S.A. Glymphatic Failure as a Final Common Pathway to Dementia*. Science.* **2020**, *370*, 50-56.
105. Holth, J.K.; Fritschi, S.K.; Wang, C.; Pedersen, N.P.; Cirrito, J.R.; Mahan, T.E.; Finn, M.B.; Manis, M.; Geerling, J.C.; Fuller, P.M. et al. The Sleep-wake Cycle Regulates Brain Interstitial Fluid Tau in Mice and CSF Tau in Humans. *Science.* **2019**, *363*, 880-884.
106. Lei, Y.; Han, H.; Yuan, F.; Javeed, A.; Zhao, Y. The Brain Interstitial System: Anatomy, Modeling, in Vivo Measurement, and Applications. *Prog Neurobiol.* **2017**, *157,* 230-246.
107. Syková, E.; Vorísek, I.; Antonova, T.; Mazel, T.; Meyer-Luehmann, M.; Jucker, M.; Hájek, M.; Ort, M.; Bures, J. Changes in Extracellular Space Size and Geometry in APP23 Transgenic Mice: A Model of Alzheimer's Disease. *Proc Natl Acad Sci U S A***. 2005**, *102*, 479-484.
108. Syková, E.; Nicholson, C. Diffusion in Brain Extracellular Space. *Physiol Rev.* **2008**, *88*, 1277-1340.
109. Thorne, R.G.; Nicholson, C. In Vivo Diffusion Analysis with Quantum Dots and Dextrans Predicts the Width of Brain Extracellular Space. *Proc Natl Acad Sci U S A.* **2006**, *103*, 5567-5572.
110. Chatterjee, K.; Carman-Esparza, C.M.; Munson, J.M. Methods to Measure, Model and Manipulate Fluid Flow in Brain. *J Neurosci Methods.* **2020**, *333*, 108541.
111. Dobson, J.; Kumar, A.; Willis, L.F.; Tuma, R.; Higazi, D.R.; Turner, R.; Lowe, D.C.; Ashcroft, A.E.; Radford, S.E.; Kapur, N. et al. Inducing Protein Aggregation by Extensional Flow. *Proc Natl Acad Sci U S A.* **2017**, *114*, 4673-4678.
112. Krishnamurthy, S.; Sudhakar, S.; Mani, E. Kinetics of Aggregation of Amyloid β Under Different Shearing Conditions: Experimental and Modelling Analyses. *Colloids Surf B Biointerfaces.* **2022**, *209*, 112156.
113. Gospodarczyk, W.; Kozak, M. Microchip Circulation Drastically Accelerates Amyloid Aggregation of 1-42 β-amyloid Peptide from Felis catus. *ACS Chem Neurosci.* **2017***, 8*, 2558-2567.
114. Bekard, I.B.; Asimakis, P.; Bertolini, J.; Dunstan, D.E. The Effects of Shear Flow on Protein Structure and Function. *Biopolymers.* **2011**, *95*, 733-745.
115. Rocha, S.; Kumar, R.; Nordén, B.; Wittung-Stafshede, P. Orientation of α-Synuclein at Negatively Charged Lipid Vesicles: Linear Dichroism Reveals Time-Dependent Changes in Helix Binding Mode. *J Am Chem Soc.* **2021**, *143*, 18899-18906.
116. Szymczak, P.; Cieplak, M. Proteins in a Shear Flow. *J Chem Phys.* **2007**, *127*, 155106.
117. Sterpone, F.; Derreumaux, P.; Melchionna, S. Molecular Mechanism of Protein Unfolding under Shear: A Lattice Boltzmann Molecular Dynamics Study*. J Phys Chem B.* **2018**, *122*, 1573-1579.

118. Languin-Cattoën, O.; Melchionna, S.; Derreumaux, P.; Stirnemann, G.; Sterpone, F. Three Weaknesses for Three Perturbations: Comparing Protein Unfolding Under Shear, Force, and Thermal Stresses. *J Phys Chem B.* **2018**, *122*, 11922-11930.
119. Languin-Cattoën, O.; Laborie, E.; Yurkova, D.O.; Melchionna, S.; Derreumaux, P.; Belyaev, A.V.; Sterpone, F. Exposure of Von Willebrand Factor Cleavage Site in A1A2A3-Fragment under Extreme Hydrodynamic Shear. *Polymers (Basel).* **2021**, *13*, 3912.
120. Hakala, T.A.; Yates, E.V.; Challa, P.K.; Toprakcioglu, Z.; Nadendla, K.; Matak-Vinkovic, D.; Dobson, C.M.; Martínez, R.; Corzana, F.; Knowles, T.P.J. et al. Accelerating Reaction Rates of Biomolecules by Using Shear Stress in Artificial Capillary Systems. *J Am Chem Soc.* **2021**, *143*, 16401-16410.
121. Brandner, F.A.; Timr, S.; Melchionna, S.; Derreumaux, P.; Baaden, M.; Sterpone, F. Modelling Lipid Systems in Fluid with Lattice Boltzmann Molecular Dynamics simulations and Hydrodynamics. *Sci Rep.* **2019**, *9*, 16450.
122. Nakamura, K.; Omori, T.; Ishikawa, T. Shear-Induced Migration of a Transmembrane Protein within a Vesicle. *Biophys J.* **2019**, *116*, 1483-1494.
123. Amador, G.J.; van Dijk, D.; Kieffer, R.; Aubin-Tam, M.E.; Tam, D. Hydrodynamic Shear Dissipation and Transmission in Lipid Bilayers. *Proc Natl Acad Sci U S A.* **2021**, *118*, e2100156118.
124. Färber, N.; Reitler, J.; Kamenac, A.; Westerhausen, C. Shear Stress Induced Lipid Order and Permeability Changes of Giant Unilamellar Vesicles. *Biochim Biophys Acta Gen Subj.* **2022**, *1866*, 130199.
125. Iida, A.; Abe, M.; Nochi, M.; Soga, C.; Unoura, K.; Nabika, H. Promoted Aggregation of Aβ on Lipid Bilayers in an Open Flowing System. *J Phys Chem Lett.* **2021**, *12*, 4453-4460.
126. Trumbore, C.N. Shear-Induced Amyloid Formation in the Brain: III. The Roles of Shear Energy and Seeding in a Proposed Shear Model. *J Alzheimers Dis.* **2018**, *65*, 47-70.
127. Melquiond, A.; Mousseau, N.; Derreumaux, P. Structures of Soluble Amyloid Oligomers from Computer Simulations. *Proteins.* **2006**, *65*, 180-191.
128. De Simone A.; Derreumaux, P. Low Molecular Weight Oligomers of Amyloid Peptides Display Beta-barrel Conformations: A Replica Exchange Molecular Dynamics Study in Explicit Solvent. *J Chem Phys.* **2010**, *132*, 165103.
129. Do, T.D.; LaPointe, N.E.; Nelson, R.; Krotee, P.; Hayden, E.Y.; Ulrich, B.; Quan, S.; Feinstein, S.C.; Teplow, D.B.; Eisenberg, D. et al. Amyloid β-Protein C-Terminal Fragments: Formation of Cylindrins and β-Barrels. *J Am Chem Soc.* **2016**, *138*, 549-557.
130. Sun, Y.; Ge, X.; Xing, Y.; Wang, B.; Ding, F. β-barrel Oligomers as Common Intermediates of Peptides Self-Assembling into Cross-β Aggregates. *Sci Rep.* **2018**, *8*, 10353.
131. Buchanan, L.E.; Maj, M.; Dunkelberger, E.B.; Cheng, P.N.; Nowick, J.S.; Zanni, M.T. Structural Polymorphs Suggest Competing Pathways for the Formation of Amyloid Fibrils That Diverge from a Common Intermediate Species. *Biochemistry.* ***2018***, *57*, 6470-6478.
132. Sun, Y.; Kakinen, A.; Wan, X.; Moriarty, N.; Hunt, C.P.J.; Li, Y.; Andrikopoulos, N.; Nandakumar, A.; Davis, T.P.; Parish, C.L. et al. Spontaneous Formation of β-sheet Nano-barrels during the Early Aggregation of Alzheimer's Amyloid Beta. *Nano Today.* **2021**, *38*, 101125.
133. Luiken, J.A.; Bolhuis, P.G. Primary Nucleation Kinetics of Short Fibril-Forming Amyloidogenic Peptides. *J Phys Chem B.* **2015**, *119*, 12568-12579.
134. Stephens, A.D.; Kaminski Schierle, G.S. The Role of Water in Amyloid Aggregation Kinetics. *Curr Opin Struct Biol.* **2019**, *58*, 115-123.
135. Doig, A.J.; Del Castillo-Frias, M.P.; Berthoumieu, O.; Tarus, B.; Nasica-Labouze, J.; Sterpone, F.; Nguyen, P.H.; Hooper, N.M.; Faller, P.; Derreumaux P. Why Is Research on

Amyloid-β Failing to Give New Drugs for Alzheimer's Disease? *ACS Chem Neurosci.* **2017**, *8*, 1435-1437.
136. Dicke, S.S.; Maj, M.; Fields, C.R.; Zanni, M.T. Metastable Intermediate during hIAPP Aggregation Catalyzed by Membranes as Detected with 2D IR Spectroscopy. *RSC Chem Biol.* **2022**, *3*, 931-940.
137. Rivas, G.; Minton, A.P. Macromolecular Crowding In Vitro, In Vivo, and In Between. *Trends Biochem Sci.* **2016**, *41*, 970-981.
138. Sterpone, F.; Derreumaux, P.; Melchionna, S. Protein Simulations in Fluids: Coupling the OPEP Coarse-Grained Force Field with Hydrodynamics. *J Chem Theory Comput.* **2015**, *11*, 1843-1853.
139. Chiricotto, M.; Melchionna, S.; Derreumaux, P.; Sterpone, F. Hydrodynamic Effects on β-amyloid (16-22) Peptide Aggregation. *J Chem Phys.* **2016,** *145*, 035102.
140. Wiesnieski, T.; Castano, E.; Ghiso, J; Frangione, B. Cerebrospinal Fluid Inhibits Alzheimer? -Amyloid Fibril Formation in Vitro, *Ann. Neurol.* **1993**, *34,* 631-633.
141. Frankel, R.; Törnquist, M.; Meisl, G.; Hansson, O.; Andreasson, U.; Zetterberg, H.; Blennow, K.; Frohm, B.; Cedervall, T.; Knowles, T.P.J. et al. Autocatalytic Amplification of Alzheimer-associated Aβ42 Peptide Aggregation in Human Cerebrospinal Fluid. *Commun Biol.* **2019**, *2*, 365.
142. Collins, S.; van Vliet, L.; Gielen, F.; Janecek, M.; Valladolid, S.W.; Poudel, C.; Fusco, G.; De Simone, A.; Michel, C.; Kaminski, C.F. et al. A Unified in Vitro to in Vivo Fluorescence Lifetime Screening Platform Yields Amyloid β Aggregation Inhibitors. bioRxiv **2022,** https://doi.org/10.1101/2022.03.28.485913
143. Löhr, T.; Kohlhoff, K.; Heller, G.T.; Camilloni, C.; Vendruscolo, M. A Small Molecule Stabilizes the Disordered Native State of the Alzheimer's Aβ Peptide. *ACS Chem Neurosci.* **2022**, *13*, 1738-1745.

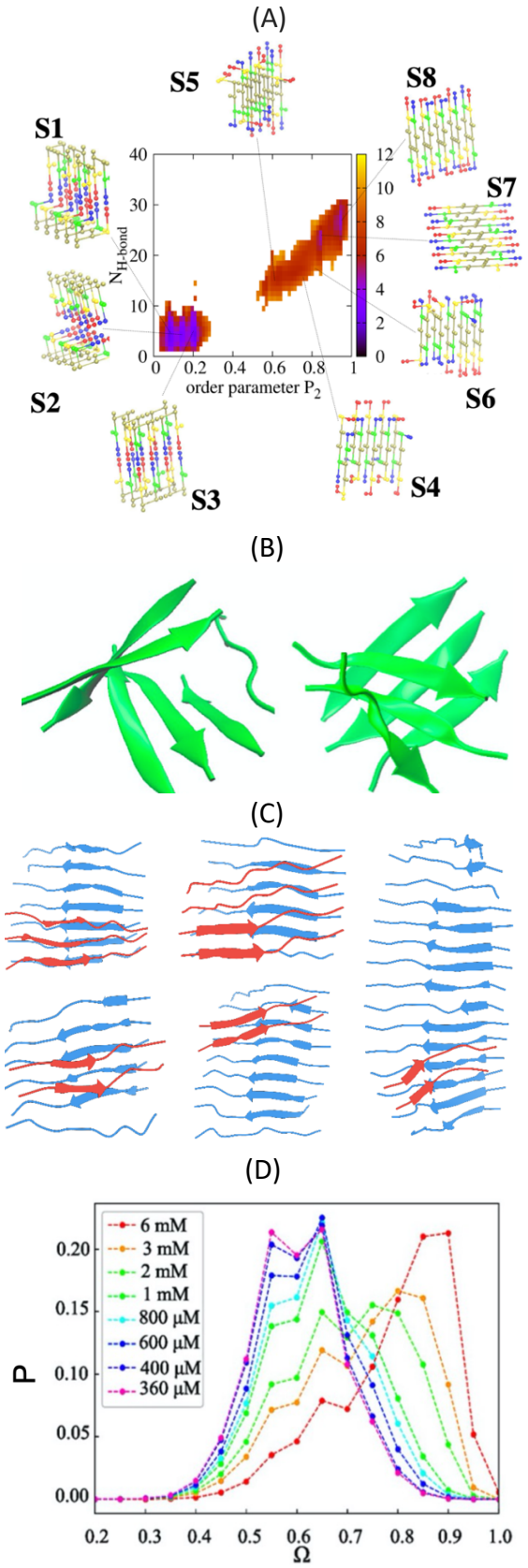

Figure 1. Free energy landscape of 10-mers Aβ37-42 as a function of P2 and N-HB (A).[7] Representative structures of Aβ16-22 aggregation nuclei (B).[14] Representative structures of transthyretin fragment primary nuclei (C).[19] Ω probability distributions of Aβ16-21 pathways at various concentrations. Perfect 1SN or 2SN pathway has Ω = 0 or 1, respectively (D).[23]

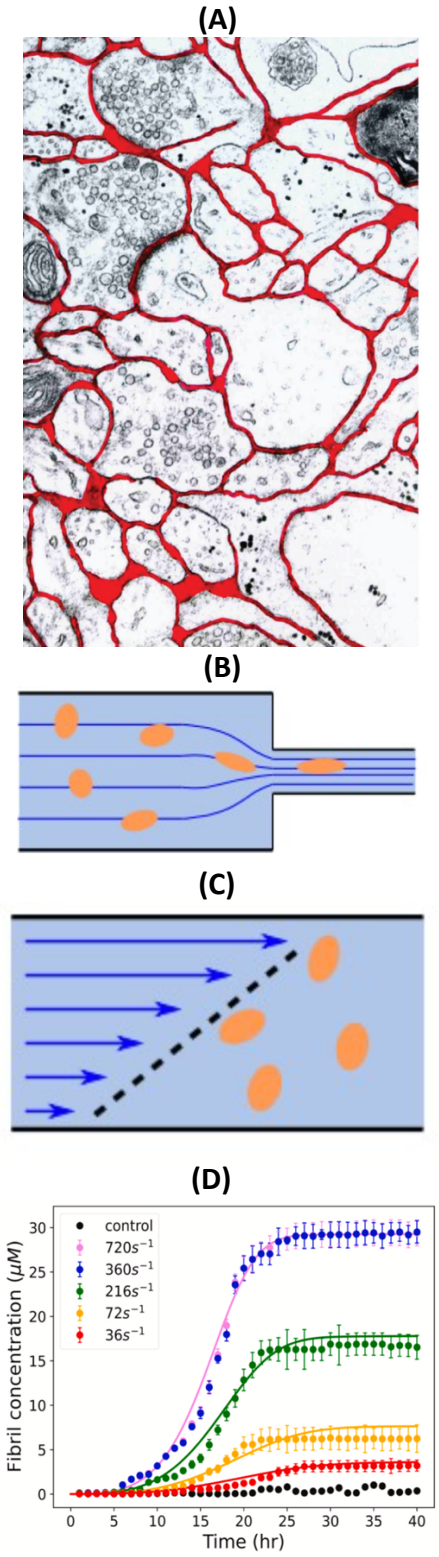

Figure 2. Electron micrograph showing a small area of cortical neuropil from the brain of a rat. The interstitial extracellular space around neurons is in red (A).[108] Schematic representation of the experimental microfluidic set up used to study BSA aggregation with blue arrows showing representing the velocity profile (B).[111] Schematic depiction of shear flows in a Couette experiment (C). Time evolution of Aβ40 fibril concentrations at different shear rates using Couette cell (D).[112]

TOC Graphic